EUROPEAN JOURNAL OF PURE AND APPLIED MATHEMATICS
2025, Vol. 18, Issue 1, Article Number 5712
ISSN 1307-5543 – ejpam.com
Published by New York Business Global

Modeling of the Euler-Poisson Equations for Rigid Bodies in the Context of the Gyrostatic Influences: An Innovative Methodology

T. S. Amer[1,*], W. S. Amer[2], M. Fakharany[1,3], A. H. Elneklawy[4], H. F. El-Kafly[5]

[1] *Department of Mathematics, Faculty of Science, Tanta University, Tanta 31527, Egypt*
[2] *Department of Mathematics and Computer Science, Faculty of Science, Menoufia University, 32511, Egypt*
[3] *Mathematics and Statistics Department, College of Science, Taibah University, Yanbu, Saudi Arabia*
[4] *Department of Mathematics, Faculty of Science, Kafrelsheikh University, Kafr El-Sheikh 33516, Egypt*
[5] *Tanta Higher Institute of Engineering and Technology, Tanta, Egypt*

Abstract. This paper presents an alternative approach to solving Euler-Poisson's dynamical equations, which describe the governing equations of how a rigid body (RGB) rotates around a stationary point with the influence of a gyrostatic moment (**GM**). The RGB's angular velocity vector components in our solution are different from those in the well-known cases. It is expected that the RGB's center of mass lies in the meridional plane along its principal axis of inertia. Additionally, it is assumed that the main inertia moments correspond to a fundamental algebraic equality. Additionally, there is a constraint on the first condition selection. The analytical solution of the problem is provided and depicted graphically using computer codes, allowing us to analyze the motion at any given time. The influence of distinct values of the **GM** on these solutions are also presented. One could consider the solution to be an entirely novel iteration of Euler's original case. Solving this equation is crucial due to its broad range of applications, including the design and development of stability enhancement systems in automobiles, dynamics-based sensors like gyroscopic sensors, the analysis of space objects and robotic systems, and gaining insight into the complex movements of RGBs.

2020 Mathematics Subject Classifications: 70E17, 70F07, 70H45, 65L05

Key Words and Phrases: Nonlinear dynamics, Rigid body, Euler-Poisson's equations, Gyrostatic moment, Exact solution

*Corresponding author.
DOI: https://doi.org/10.29020/nybg.ejpam.v18i1.5712

Email addresses: tarek.saleh@science.tanta.edu.eg (T. S. Amer), drwaelamer@science.menofia.edu.eg (W. S. Amer), mohamed.elfakharany@science.tanta.edu.eg and fakharany@aucegypt.edu (M. Fakharany), ahmed_hassan@sci.kfs.edu.eg (A. H. Elneklawy), heba_elkafly@yahoo.com (H. F. El-Kafly)

1. Introduction

The phenomenon of the RGB's rotational movement around a stationary point stands as a significant inquiry within theoretical mechanics. This particular problem has garnered the attention of numerous researchers over the past fifty years, as evidenced by various studies [1–7, 9–13, 17, 19–25, 27–34]. The research topic holds immense significance owing to its extensive range of applications in the field of mechanics. In order to address these challenges, intricate techniques need to be employed as they are controlled by a system that comprises six non-linear differential equations (DEs), in addition to three first integrals [13, 28, 34]. In [30], the authors explore the solution for disturbed rotational movements of the RGB, reminiscent of the conventional precession observed in Lagrange's scenario. This particular investigation focuses on cases where the restoring torque relies on the angle of nutation. The authors employ both the small parameter and averaging techniques to deduce averaged equations of motion (EOM). In [29], a similar approach for the perturbed rotational motion of the RGB possessing an almost Lagrangian mass distribution is studied. In [25], a novel method is presented to describe the rotational behavior of an asymmetric RGB by leveraging the moment of momentum vector. It is emphasized that there is a similarity in the rotational behavior of an asymmetric RGB when it experiences a moment along its axis of symmetry and when it is subjected to a continuous variation of moment. Moreover, a precise solution is obtained for the given problem by accounting for the impact of linear viscous friction. In [24], the motion of the RGB around a fixed point subject to the effects of a Newtonian field (NF) is examined. Euler-Poisson's equations are utilized to describe this movement. These equations have three first integrals that are widely recognized. The authors have shown that by defining the necessary and sufficient conditions, it becomes possible to identify functions that can represent the fourth first integral of the EOM.

The authors have discovered that by determining the necessary and sufficient conditions, it is possible to identify certain functions that can serve as the fourth first integral for the governing equations. In [4], the analytical solutions for Euler's equations governing the motion of a RGB are presented. Specifically, the focus is on a scenario where the body is fixed at a point and subjected to a gyrostatic torque. By considering the inherent physical characteristics of the body, the analytical solutions are derived. Furthermore, the uniqueness of these solutions has been established and proven. In [17], a novel and precise solution to Euler's equations has been introduced. This groundbreaking solution demonstrates notable distinctions in all aspects of the angular velocity of the RGB compared to both symmetric rigid rotors and Euler's case when no torques are applied, as well as other widely recognized specific scenarios. Additionally, this solution has been mathematically proven to adhere to Euler-Poinsot's equations, encompassing motion invariants and an additional invariant specific to Euler's principles. In [1] corresponding to previous studies [29, 30], a study that examines the effects of a central NF on a gyrostat is presented. This field originates from an attracting center positioned along a downward fixed axis. The study also delves into the third component of the **GM** vector, along with the effects of the restoring moment and the perturbing moment vector.

In [3], a different research study focuses on the movement of a symmetrical RGB along one of its primary axes. This study explores the impact of the NF in conjunction with a gyrostatic torque, where the second component of this torque is considered null. In [2], the author presents a novel solution for Lagrange's equation in the case of the dynamical behavior of the RGB suspended on an elastic spring as a pendulum model. In [23], the effects of a gyrostatic torque with both its first and second components set to zero, along with the NF, are investigated. In [5], the main subjects of study are the motion of an asymmetric RGB under the influence of the NF, gyrostatic torque, and perturbing moments. In [33], a study investigates the most efficient way to slow down a dynamically asymmetric RGB by employing nondimensional variables. This approach allows for the derivation of a system of motion equations with multiple parameters. By constructing a vector hodograph of the angular momentum in three-dimensional space, various combinations of system parameters are explored. The Krylov-Bogoliubov-Mitropolski asymptotic averaging method, as described in [27, 31, 32], is utilized to study the movement of RGBs that contain fluid-filled cavities and are influenced by the **GM** vector. By adjusting a small parameter for the second approximation, the authors successfully derive the governing equation of motion in its standardized form. They then conducted an analysis of the Cauchy problem for a system that was identified through the averaging process. In [21], another investigation on the motion of the RGB, which experiences a restoring moment, a third **GM** component, and a perturbing moment, is presented. In [19], the impact of a **GM**, constant torques along the axes connected to the body, and resistant forces on the movement of a charged RGB are discussed. In [20], the examination of the RGB in three-dimensional space with a smooth surface of any shape has been explored. This body is immersed in an unbounded liquid and subjected to a predetermined external force and constant torques that are fixed to the body. It is demonstrated that there exists at least one comprehensive and stable solution to the initial boundary value problem related to this case, provided the input data are regular and small enough, and the external force and constant torques applied to the body decrease gradually. In [22], an examination is carried out on recurrent patterns of motion in a connected gyrostat with a spring. This gyrostat is influenced by a **GM** vector, along with the forces from an NF and a magnetic one. The study's outcomes also include the formulation of solutions and the generation of phase diagrams, which vividly illustrate the periodicity and stability properties of the solutions. In [6–12], the authors approach a solution for Euler's equation for the RGB's motion under external torques. In [11], the solutions for the angular velocities correspond to three constant torque scenarios related to the major, minor, and middle axes case. In [10], in addition to the solutions for the angular velocities, a solution for Euler angles, transverse and axial velocities, and displacement are presented. In [9], the solution is presented related to time-varying transverse torques and constant axial torque. In [7], the solution is approached for a nearly symmetric model for the RGB with constant torques and the **GM**. In [12], the Krylov-Bogoliubov-Mitropolski method is used to approach the solution for the motion of the RGB about a fixed point in which the ellipsoid of inertia is close to the ellipsoid of rotation. In [6], Euler-Poisson equations are solved through the utilization of Poincaré's small parameter method along with its adaptations when the

scenario of irrational frequencies is considered. In [8], Euler's equation is solved for the case of a RGB, which is supposed to have a chamber with a globular shape, in which it contains a moving mass and is filled with a viscous liquid. A new method for solving the dynamics equations of a charged particle is presented in [14]. This study utilized a new procedure across all these equations, including the momentum equation for charged particle dynamics governed by the Lorentz force in a non-relativistic framework. A novel method for solving the EOM for a satellite in trapped orbits is presented in [16]. In the case of the elliptic restricted three-body problem, the satellite is ensnared in a spatial trap and moves in close proximity to the planet. In order to determine the coordinates of a satellite with an orbit close to the planet, a novel kind of solving process is used here. The system of EOM was utilized to achieve the analytic and semi-analytical solutions. In [15, 18], the analytical approach to the study of mathematical models in applications to various non-linear problems in celestial mechanics, along with the dynamics of RGB rotation, has been presented. The author drew our attention to an approach to solving the dynamic motion of celestial bodies like asteroids, which will be considered in our future work.

This study explores the dynamical behavior of a RGB influenced by a **GM**. It is assumed that the RGB's center of mass lies in the meridional plane along its inertia principal axis. By incorporating certain algebraic assumptions about moments of inertia, we arrive at the obtained solution. The subsequent sections of this paper visually depict this solution to illustrate the behavior of the body's motion within the **GM**. As a result, this study can be seen as a new modification of Euler's framework concerning the motion of RGBs under external torques. Researchers may acquire a better understanding of the conservation and equilibrium of angular momentum in computational physics and mechanical engineering by solving Euler's equations, particularly in situations where objects are affected at both microscopic and tiny scales by external fields such as electromagnetic, Newtonian, or gravitational fields. Control, transportation, and stabilization of satellites depend on proper satellite rotation modeling, which is made possible by the resulting solution of Euler's equations in the aerospace industry. Designers may develop manipulators and mobile robots with precise movement by understanding how rigid things rotate.

2. The Controlling Equation of Motion

Let's begin by examining the rotatory movement of a heavy RGB of mass M that revolves around a stationary point O inside the RGB under the implications of a **GM** vector whose components are ℓ_1, ℓ_2, and ℓ_3. Let's take into consideration two frames respected to the body: $OXYZ$ is the fixed frame while $Oxyz$ is the rotating frame, and they are stationed at the origin O. Suppose that (p, q, r) symbolize the projections of the RGB's angular velocity on the inertia's main axes and $\hat{\gamma} = (\gamma_1, \gamma_2, \gamma_3)$ corresponds to the directed unit vector on the fixed Z-axis as revealed in Figure 1. The controlling EOM are

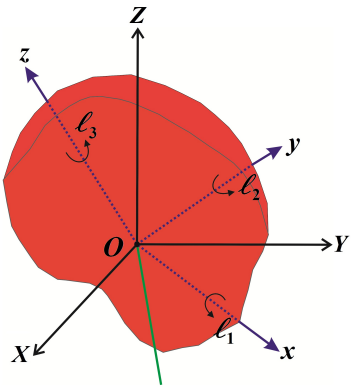

Figure 1: The simulation of RGB's model.

expressed below [17, 34]

$$\begin{aligned} A\dot{p} + (C-B)qr + \ell_3 q - \ell_2 r &= Mg(\gamma_2 z_0 - \gamma_3 y_0), \\ B\dot{q} + (A-C)rp + \ell_1 r - \ell_3 p &= Mg(\gamma_3 x_0 - \gamma_1 z_0), \\ C\dot{r} + (B-A)pq + \ell_2 p - \ell_1 q &= Mg(\gamma_1 y_0 - \gamma_2 x_0), \end{aligned} \tag{1}$$

with

$$\dot{\gamma}_1 = r\gamma_2 - q\gamma_3, \quad \dot{\gamma}_2 = p\gamma_3 - r\gamma_1, \quad \dot{\gamma}_3 = q\gamma_1 - p\gamma_2, \tag{2}$$

where (A, B, C) represent the RGB's main inertia moments, g is the acceleration due to the gravity, $\mathbf{r}_0 = (x_0, y_0, z_0)$ is the mass center position vector in the coordinates $Oxyz$, the over-dot denotes the derivative with respect to time. Equations (1) and (2) have the first integrals, given by

$$\begin{aligned} \gamma_1^2 + \gamma_2^2 + \gamma_3^2 &= 1, \\ (Ap + \ell_1)\gamma_1 + (Bq + \ell_2)\gamma_2 + (Cr + \ell_3)\gamma_3 &= C_0, \\ Ap^2 + Bq^2 + Cr^2 + 2Mg(x_0\gamma_1 + y_0\gamma_2 + z_0\gamma_3) &= 2C_1, \end{aligned} \tag{3}$$

where C_0, and C_1 are integral constants.

3. Euler's Case

Similar to Euler's case, we acquire the subsequent fourth first integral based on the existence of the **GM**

$$Ap^2 + Bq^2 + Cr^2 + 2\ell_1(B-C)qr + 2\ell_2(C-A)rp + 2\ell_3(A-B)pq = -C_0^2. \tag{4}$$

By leveraging the first two integrals presented in (3) and the fourth integral (4), one gets

$$\gamma_1 = \frac{Ap + \ell_1}{C_0}, \qquad \gamma_2 = \frac{Bq + \ell_2}{C_0}, \qquad \gamma_3 = \frac{Cr + \ell_3}{C_0}. \tag{5}$$

Upon substituting systems (1) and (2) into the third equation in the system (3), we obtain

$$\frac{1}{C_3}\left(C(A-C)r^2 + B(A-B)q^2\right) + Apx_0 + Bqy_0 + Crz_0 = C_2, \tag{6}$$

where

$$C_2 = C_0\left[\frac{C_1}{Mg} - \frac{C_0}{2AMg} - \frac{1}{C_0}\left(x_0\ell_1 + y_0\ell_2 + z_0\ell_3\right)\right], \quad C_3 = \frac{2AMg}{C_0}.$$

Equation (6) demonstrates a linear combination of the first integrals (3), the fourth integral (4), and (5). Consequently, our aim is to determine a solution that complies with the stated equation (6).

4. The Enhanced Solution at $x_0 = 0$

Considering our perspective, let us collectively examine the subsequent option in conjunction with $z_0 \neq 0$,

$$\left(\frac{y_0}{z_0}\right)^2 = \frac{C(B-A)}{B(A-C)}. \tag{7}$$

Besides that, let us choose $x_0,\ C_2 = 0$ in equation (6). The condition $C_2 = 0$ implies

$$C_0^2 = 2AC_1 - C_3(x_0\ell_1 + y_0\ell_2 + z_0\ell_3).$$

In such case, equation (6) is expressed as

$$Bqy_0 + Crz_0 = \left[q\sqrt{\frac{B(B-A)}{C_3}} - r\sqrt{\frac{C(A-C)}{C_3}}\right]\left[q\sqrt{\frac{B(B-A)}{C_3}} + r\sqrt{\frac{C(A-C)}{C_3}}\right].$$

Hence, the aforementioned equalities (6) hold given the specified conditions (7), and the last algebraic equation can be simplified as

$$q\sqrt{\frac{B(B-A)}{C_3}} + r\sqrt{\frac{C(A-C)}{C_3}} = 0 \Rightarrow r = \frac{By_0}{Cz_0}q.$$

Taking into consideration equation (3), one obtains

$$q = \frac{z_0}{B}\sqrt{\frac{C_0^2 - A^2p^2}{y_0^2 + z_0^2}}, \quad r = \frac{y_0}{C}\sqrt{\frac{C_0^2 - A^2p^2}{y_0^2 + z_0^2}}. \tag{8}$$

Afterward, by replacing the equalities (8) with the system (1), one can deduce that each of them holds given the conditions (7). Additionally, every equation in (1) needs to be simplified into the individual ordinary differential equation presented below

$$\frac{dp}{dt} = \Gamma_1(C_0^2 - A^2p^2) + \Gamma_2\sqrt{C_0^2 - A^2p^2} + \Gamma_3,$$

where

$$\Gamma_1 = \frac{(C-A)y_0}{CA^2z_0}, \quad \Gamma_2 = \left[\frac{Mg}{C_0} - \frac{1}{y_0^2 + z_0^2}\left(\frac{y_0\ell_2}{C} + \frac{z_0\ell_3}{B}\right)\right]\frac{\sqrt{y_0^2 + z_0^2}}{A}, \quad \Gamma_3 = \frac{Mg}{AC_0}(z_0\ell_2 - y_0\ell_3).$$

Separating variables and integrating both sides, yields

$$\int \frac{dp}{\Gamma_1(C_0^2 - A^2p^2) + \Gamma_2\sqrt{C_0^2 - A^2p^2} + \Gamma_3} = \int dt. \tag{9}$$

Considering $A > B > C,\ z_0 \neq 0$ implies $\Gamma_1 = \frac{(C-A)y_0}{CA^2z_0}$, and $\Gamma_2 = \frac{Mg}{AC_0}\sqrt{y_0^2 + z_0^2}$. Thus, the solution to equation (9) for p is represented by the appropriate elliptical integral [26]. Furthermore, it is important to highlight that the utilization of Euler's invariant (3) leads to the establishment of a suitable restriction for equations (8) and (9) as $C_0^2 - A^2p^2 > 0$.

5. The Exact solution at $x_0 = z_0 = 0$

Let's choose the case $x_0 = z_0 = 0$ in (6) which gives

$$r^2 = \frac{C_2C_3 + B(B-A)q^2 - BC_3y_0q}{C(A-C)}; \quad A \neq C, \tag{10}$$

from equation (3), one obtains

$$p^2 = \frac{C_0^3 - 2CC_0C_1 + 2MgC(x_0\ell_1 + y_0\ell_2 + z_0\ell_3)}{A(A-C)C_0} + \frac{2MgBCy_0}{A(A-C)C_0}q - \frac{B(B-C)}{A(A-C)}q^2; \quad A \neq C. \tag{11}$$

Afterwards, by replacing equalities (10) and (11) into the system of equation (1), we can deduce that every one of them holds. Furthermore, each equation in (1) needs to be simplified into a singular ordinary differential equation, as shown below

$$\int \left(\sqrt{f_1(q,q^2)f_2(q,q^2)} - \frac{\ell_1\sqrt{f_1(q,q^2)} - \ell_3\sqrt{f_2(q,q^2)}}{\sqrt{B(A-C)}} \right)^{-1} dq = -\int dt; \quad A \neq C, \tag{12}$$

where

$$f_1(q,q^2) = \frac{2AC_0C_1 - C_0^3 - 2AMgy_0\ell_2}{BCC_0} - \frac{2AMgy_0}{CC_0}q + \frac{B-A}{C}q^2,$$
$$f_2(q,q^2) = \frac{C_0^3 - 2CC_0C_1 + 2MCgy_0\ell_2}{ABC_0} + \frac{2MCgy_0}{AC_0}q + \frac{B-C}{A}q^2,$$
$$f_1(q,q^2)f_2(q,q^2) > 0.$$

Therefore, the final solution of (12) for q is given by the proper elliptical integral [26].

6. Results Discussion

In this section, we aim to present a graphic collection of numerical outcomes for the obtained solutions through a computer program. The subsequent data will be utilized to ascertain the movement within the problem under consideration

$$A = 100\text{kg.m}^2, \quad B = 80\text{kg.m}^2, \quad C = 70\text{kg.m}^2, \quad M = 300\text{kg}, \quad g = 9.8\text{m/s}^2,$$
$$\ell_i = (10, 30, 50)\text{kg.m}^2\text{.s}^{-1}, \quad i = 1, 2, 3.$$

Fig.2 displays the variation of the components p, q, and r with time t when the value of the first component of the **GM** varies as $\ell_1 = (10, 30, 50)\text{kg.m}^2\text{.s}^{-1}$, while the other two components ℓ_2, ℓ_3 remain fixed at $10\text{kg.m}^2\text{.s}^{-1}$. In Fig.(2a), the red curve starts from an initial value close to 0 and gradually increases until it plateaus at around 20. The curve reaches its maximum faster in the beginning, then slows down as it approaches its final value. The blue curve shows a similar behavior, but it starts from a higher initial value, eventually stabilizing near 30. This curve also increases rapidly in the beginning and then slows as it approaches its final value. The black curve starts even higher and stabilizes around 50. Like the other two, it rapidly grows at the start and then slows down as it levels off. As the value of ℓ_1 increases, the steady-state value of p also increases. This indicates that the angular velocity component p grows proportionally to the applied torque and stabilizes over time. In Fig.(2b), the red curve starts negative and rapidly decreases to approximately -50, stabilizing after a short period. The blue curve also decreases rapidly, but it stabilizes at a more negative value (around -100). The black curve stabilizes at the most negative value, around -150, after an initial rapid decrease. The angular velocity component q decreases and stabilizes at increasingly negative values as the gyrostatic torque ℓ_1 increases, which suggests a relationship where a stronger torque leads to a higher magnitude (in the negative direction) of q. In Fig.(2c), the red curve starts from a higher value around 0.6 and gradually decreases over time until it nearly reaches zero. The blue curve starts higher than the red one and also decreases rapidly, stabilizing close to zero. The black curve begins from the highest initial value and then follows a similar trend, rapidly decreasing and stabilizing near zero. The angular velocity component r starts higher for larger values of ℓ_1, but all curves eventually approach zero. This behavior shows that r tends to decay over time and reach a small or negligible value, regardless of the torque, but stronger torques cause it to initially start at higher values. Consequently, increasing the gyrostatic torque changes the final steady-state values of p, q, and r and the rate at which they reach their steady states.

Fig.3 expresses the variance in the body's angular velocity p, q and r via time t for several values of the second component of the **GM**; $\ell_2 = 10, 30, 50\text{kg.m}^2\text{.s}^{-1}$, meanwhile the other two components remain constat $\ell_1 = \ell_3 = 10$ $\text{kg.m}^2\text{.s}^{-1}$. In Fig.(3a), the red curve starts from an initial low value and gradually increases to about 20. The blue curve starts higher than the red curve and stabilizes around 30. The black curve begins from the highest value and stabilizes near 50. This behavior is similar to the previous set of graphs for p. As ℓ_2 increases, the final stable value of p also increases. This suggests a similar dependency of p on ℓ_2, where p increases with the strength of ℓ_2. In Fig.(3b), the red curve decreases and stabilizes around -50. The blue curve decreases more and stabilizes around -100. The black curve decreases even further, stabilizing around -150. Like the previous graphs, q decreases and reaches increasingly negative steady-state values as ℓ_2 increases. The stronger the torque ℓ_2, the more negative the final steady-state value of q . In Fig.(3c), the red curve starts at around 0.6 and decreases toward zero. The blue curve starts from a slightly higher value than the red curve and decreases rapidly. The black curve starts from the highest value and decreases faster than the others, stabilizing

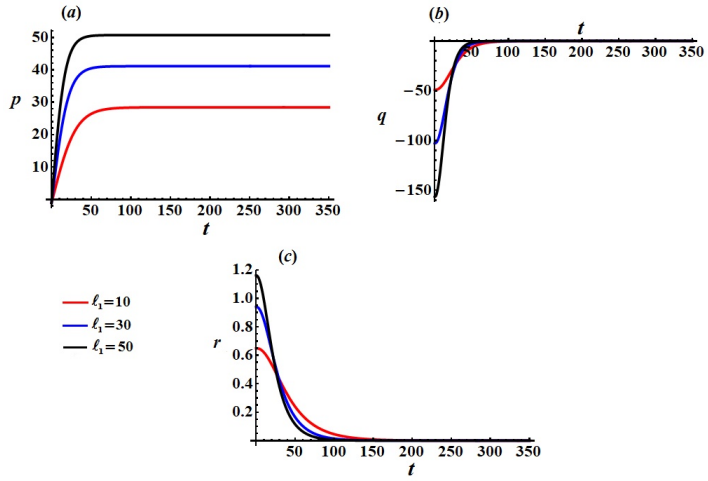

Figure 2: Presents the time-dependent change of p, q, and r when $\ell_1 = (10, 30, 50)\text{kg.m}^2\text{.s}^{-1}$, while $\ell_2, \ell_3 = 10\text{kg.m}^2\text{.s}^{-1}$.

near zero. The angular velocity component r starts at a higher value when ℓ_2 is larger but decays toward zero in all cases. Similar to the previous set, r shows an initial dependence on ℓ_2 but eventually decreases toward a negligible value for all values of ℓ_2. The consistency between the two sets of graphs for ℓ_1 and ℓ_2 suggests that both torque components (ℓ_1 and ℓ_2) influence the system similarly, at least in terms of the time evolution of p, q, and r. This suggests that these angular velocity components are primarily influenced by the magnitude of the torque applied, whether it is ℓ_1 and ℓ_2.

Fig.4 shows the temporal change of p, q and r when the value of the third component of the **GM** varies as $\ell_3 = 10, 30, 50\text{kg.m}^2\text{.s}^{-1}$, whereas the other two components remain constat $\ell_1 = \ell_2 = 10$ kg.m^2.s^{-1}. In Fig.(4a), the red curve increases rapidly and stabilizes around 25. The rise is steep at the beginning and levels off as time progresses. The blue curve follows a similar pattern but stabilizes around 20, showing a slower increase compared to the red curve. The black curve increases even more slowly and stabilizes around 15. Here, p behaves differently from the previous graphs. The smaller the value of ℓ_2, the larger the steady-state value of p. This contrasts with previous graphs where larger values of torque produced larger final values of p, which indicates an inverse relationship between p and ℓ_2. In Fig.(4b), the red curve decreases rapidly to around -50, then recovers, crossing over into positive values, stabilizing around 0. The blue curve decreases similarly but recovers more gradually, leveling off at a value slightly below 0. The black curve decreases less sharply than the others and eventually stabilizes around -10. The angular velocity component q shows some oscillatory recovery after an initial drop, especially in the case of $\ell_3 = 10\text{kg.m}^2\text{.s}^{-1}$. This contrasts with previous behaviors where q continuously decreased to a negative steady state. Here, the smaller ℓ_3 induces a recovery in q, while larger values stabilize q at more negative values. In Fig.(4c), the red curve starts at around 0.6 and decays quickly toward zero. The blue curve begins at the least value and decays more slowly toward zero. The black curve starts at an even lower value and decays to nearly

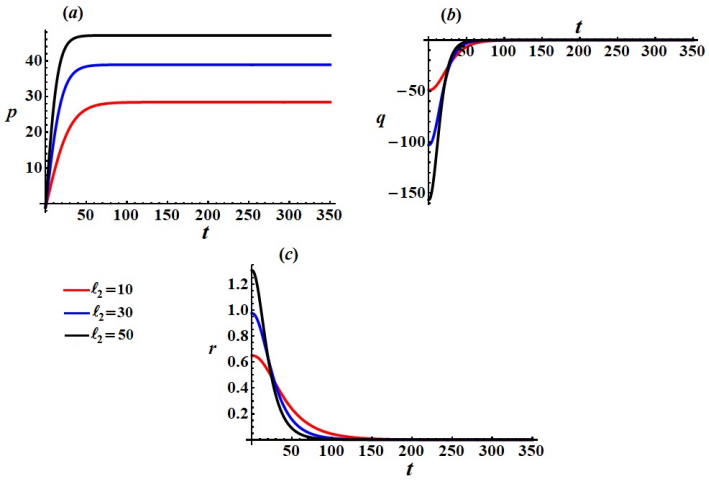

Figure 3: Depicts the time-dependent change of p, q, and r when $\ell_2 = (10, 30, 50)\text{kg.m}^2\text{.s}^{-1}$, while $\ell_1, \ell_3 = 10\text{kg.m}^2\text{.s}^{-1}$.

zero more gradually. The angular velocity component r decays towards zero, and the rate of decay is slower for larger values of ℓ_3. This is similar to the previous graphs, where r eventually decays to zero, with larger values of torque leading to a more gradual decay. These results suggest that ℓ_3 influences the system differently than ℓ_1 and ℓ_2, possibly reflects the distinct role of each component of the **GM** in the evolution of the angular velocity components.

7. Conclusion

In this study, we have created an altered solution (8), and (9) for Euler's equations (1) using Poisson's equations (2) with the consideration of a **GM** affecting the rotation of the RGB. The resulting angular velocity components differ from those in Lagrange's case, Kovalevskaya's case, Euler's case, or any other specific scenario. A limitation is placed on the selection of initial conditions for the body's variables based on the interpretation of C_0^2. The obtained solution is regarded as a modification of both Euler's case and Ershkov's study [17] when the **GM** vector is no longer significant or is absent. Various plots are graphed to illustrate the behavior of the achieved results. The numerical findings have demonstrated the significant influence of the vector of **GM** on the RGB's motion. However, the analytical results concerning the rotational motion of a rigid body around a fixed point have practical applications in industries, including satellites, autopilots, and aircraft.

Authors Statements

T. S. Amer: Investigation, Methodology, Data curation, Conceptualization, Validation, Reviewing and Editing.
W. S. Amer: Conceptualization, Resources, Formal Analysis, Validation, Visualization

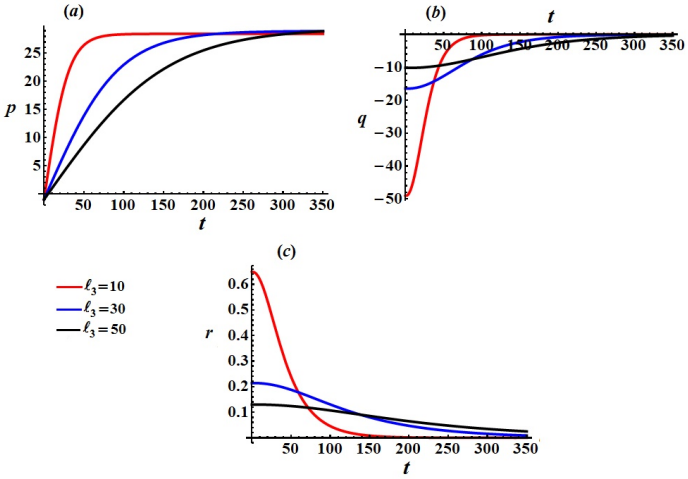

Figure 4: Shows the time-dependent change of p, q, and r when $\ell_2 = (10, 30, 50)\text{kg.m}^2\text{.s}^{-1}$, while $\ell_1, \ell_2 = 10\text{kg.m}^2\text{.s}^{-1}$.

and Reviewing.
M. Fakharany: Resources, Methodology, Validation, Formal Analysis, Conceptualization and Reviewing.
A. H. Elneklawy: Methodology, Conceptualization, Data curation, Validation, Writing-Original draft preparation.
H. F. El-Kafly: Resources, Methodology, Conceptualization, Validation, Formal Analysis, Visualization and Reviewing.

Conflict of Interest

The authors declare that they have no conflict of interest.

Funding Acknowledgement

This research received no specific grant from any funding agency in the public, commercial, or not-for-profit sectors.

Data Availability

Data sharing is not applicable to this article as no datasets were generated or analyzed during the current study.

References

[1] TS Amer. New treatment of the perturbed motions of a rotating symmetric gyrostat about a fixed point. *Thai J. Math*, 7(1):151–170, 2009.

[2] TS Amer. The dynamical behavior of a rigid body relative equilibrium position. *Advances in Mathematical Physics*, 2017(1):8070525, 2017.

[3] TS Amer. On the dynamical motion of a gyro in the presence of external forces. *Advances in Mechanical Engineering*, 9(2):1687814017691736, 2017.

[4] TS Amer and IM Abady. Solutions of euler's dynamic equations for the motion of a rigid body. *Journal of Aerospace Engineering*, 30(4):04017021, 2017.

[5] TS Amer and IM Abady. On the motion of a gyro in the presence of a newtonian force field and applied moments. *Mathematics and Mechanics of Solids*, 23(9):1263–1273, 2018.

[6] TS Amer, IM Abady, HA Abdo, and HF El-Kafly. The asymptotic solutions for the motion of a charged symmetric gyrostat in the irrational frequency case. *Scientific Reports*, 14(1):16662, 2024.

[7] TS Amer, Elneklawy AH, and El-Kafly HF. A novel approach to solving euler's nonlinear equations for a 3dof dynamical motion of a rigid body under gyrostatic and constant torques. *Journal of Low Frequency Noise, Vibration and Active Control*, page 14613484241293859, 2024.

[8] TS Amer, WS Amer, M AL Nuwairan, and HF Elkafly. Evaluating the motion of a charged solid body having a globular cavity. *Alexandria Engineering Journal*, 104:85–94, 2024.

[9] TS Amer, HF El-Kafly, AH Elneklawy, and WS Amer. Modeling analysis on the influence of the gyrostatic moment on the motion of a charged rigid body subjected to constant axial torque. *Journal of Low Frequency Noise, Vibration and Active Control*, 43(4):1593–1610, 2024.

[10] TS Amer, HF El-Kafly, AH Elneklawy, and AA Galal. Analyzing the dynamics of a charged rotating rigid body under constant torques. *Scientific Reports*, 14(1):9839, 2024.

[11] TS Amer, HF El-Kafly, AH Elneklawy, and AA Galal. Analyzing the spatial motion of a rigid body subjected to constant body-fixed torques and gyrostatic moment. *Scientific Reports*, 14(1):5390, 2024.

[12] TS Amer, AM Farag, and WS Amer. The dynamical motion of a rigid body for the case of ellipsoid inertia close to ellipsoid of rotation. *Mechanics Research Communications*, 108:103583, 2020.

[13] Felix L Chernousko, Leonid D Akulenko, and Dmytro D Leshchenko. *Evolution of motions of a rigid body about its center of mass*. Springer, 2017.

[14] Sergey Ershkov and Dmytro Leshchenko. Solving procedure for the dynamics of charged particle in variable (time-dependent) electromagnetic field. *Zeitschrift für angewandte Mathematik und Physik*, 71:1–8, 2020.

[15] Sergey Ershkov, Dmytro Leshchenko, and Alla Rachinskaya. Note on the trapped motion in er3bp at the vicinity of barycenter. *Archive of Applied Mechanics*, 91(3):997–1005, 2021.

[16] Sergey Ershkov and Alla Rachinskaya. Semi-analytical solution for the trapped orbits of satellite near the planet in er3bp. *Archive of Applied Mechanics*, 91:1407–1422, 2021.

[17] Sergey V Ershkov. New exact solution of euler's equations (rigid body dynamics) in the case of rotation over the fixed point. *Archive of Applied Mechanics*, 84:385–389, 2014.

[18] SV Ershkov and RV Shamin. On metallic-type asteroid rotation moving in magnetic field (introducing magnetic second-grade yorp effect). *Acta Astronautica*, 224:195–201, 2024.

[19] AA Galal, TS Amer, AH Elneklawy, and HF El-Kafly. Studying the influence of a gyrostatic moment on the motion of a charged rigid body containing a viscous incompressible liquid. *The European Physical Journal Plus*, 138(10):1–13, 2023.

[20] Giovanni P Galdi. Large-time behavior of a rigid body of arbitrary shape in a viscous fluid under the action of prescribed forces and torques. *Journal of Mathematical Fluid Mechanics*, 25(3):43, 2023.

[21] Ji-Huan He, TS Amer, WS Amer, HF Elkafly, and AA Galal. Dynamical analysis of a rotating rigid body containing a viscous incompressible fluid. *International Journal of Numerical Methods for Heat & Fluid Flow*, 33(8):2800–2814, 2023.

[22] Abdelaziz I Ismail, Tarek S Amer, and Wael S Amer. Advanced investigations of a restricted gyrostatic motion. *Journal of Low Frequency Noise, Vibration and Active Control*, 42(3):1205–1221, 2023.

[23] Abdelaziz I Ismail and TS Amer. The fast spinning motion of a rigid body in the presence of a gyrostatic momentum ℓ_3. *Acta mechanica*, 154(1):31–46, 2002.

[24] AI Ismail and Tarek S Amer. A necessary and sufficient condition for solving a rigid body problem. *Technische Mechanik-European Journal of Engineering Mechanics*, 31(1):50–57, 2011.

[25] EA Ivanova. A new approach to the solution of some problems of rigid body dynamics. *ZAMM-Journal of Applied Mathematics and Mechanics/Zeitschrift für Angewandte Mathematik und Mechanik: Applied Mathematics and Mechanics*, 81(9):613–622, 2001.

[26] Derek F LAWDEN. *Elliptic functions and applications*, volume 80. 1989.

[27] D Lechehenko and T Kozachenko. Evolution of rotational motions in a resistive medium of a nearly dynamically spherical gyrostat subjected to constant body-fixed torques. 2022.

[28] Eugene Leimanis. *The general problem of the motion of coupled rigid bodies about a fixed point*, volume 7. Springer Science & Business Media, 2013.

[29] DD Leshchenko. On the evolution of rigid-body rotations. *International Applied Mechanics*, 35(1):93–99, 1999.

[30] DD Leshchenko and SN Sallam. Perturbed rotational motions of a rigid body similar to regular precession. *Journal of Applied Mathematics and Mechanics*, 54(2):183–190, 1990.

[31] Dmytro Leshchenko, Sergey Ershkov, and Tetiana Kozachenko. Evolution of rotational motions of a nearly dynamically spherical rigid body with cavity containing a viscous fluid in a resistive medium. *International Journal of Non-Linear Mechanics*, 142:103980, 2022.

[32] Dmytro Leshchenko, Sergey Ershkov, and Tetiana Kozachenko. Perturbed rotational

motions of a nearly dynamically spherical rigid body with cavity containing a viscous fluid subject to constant body fixed torques. *International Journal of Non-Linear Mechanics*, 148:104284, 2023.

[33] AL Rachinskaya and EA Rumyantseva. Optimal deceleration of a rotating asymmetrical body in a resisting medium. *International Applied Mechanics*, 54(6):710–717, 2018.

[34] Hamad M Yehia. *Rigid Body Dynamics*. Springer, 2022.